Applied Catalysis B: Environmental 84 (2008) 356–362

Contents lists available at ScienceDirect

Applied Catalysis B: Environmental

journal homepage: www.elsevier.com/locate/apcatb

The effect of particle shape on the activity of nanocrystalline TiO_2 photocatalysts in phenol decomposition

Nándor Balázs [a], Károly Mogyorósi [a], Dávid F. Srankó [a], Attila Pallagi [a], Tünde Alapi [a], Albert Oszkó [b], András Dombi [a], Pál Sipos [a,*]

[a] University of Szeged, Department of Inorganic and Analytical Chemistry, Research Group for Environmental Chemistry, ReGECh, H-6701 Szeged, PO Box 440, Hungary
[b] University of Szeged, Department of Solid State and Radiochemistry, H-6701 Szeged, PO Box 168, Hungary

ARTICLE INFO

Article history:
Received 18 January 2008
Received in revised form 10 April 2008
Accepted 12 April 2008
Available online 24 April 2008

Keywords:
Titania
Anatase
Rutile
Nanoparticles
Phenol decomposition
Photocatalysis
TEM
SEM
HRTEM
Powder XRD
Specific surface area
Flame hydrolysis
Shape dependence

ABSTRACT

Nanosized TiO_2 photocatalysts were synthesized via hydrogen–air flame hydrolysis. X-ray diffraction (XRD) measurements revealed that the TiO_2 samples thus prepared consisted mainly of anatase (79–98 wt%) and the rest is rutile. Average particle diameters from TEM measurements were found to vary between 48 and 63 nm. The specific surface area of the samples was found to be practically independent of the synthesis parameters employed (20–32 $m^2 g^{-1}$). Photocatalytic activity of the catalysts was studied by using various model compounds. In spite of their very similar properties, the initial decomposition rate of phenol and methanol showed up to threefold variations within the series of the samples, and it was significantly higher for the best catalyst than that determined for Degussa P25. Our TEM measurements demonstrated that in the less active catalysts the dominant morphology of the particles is spherical, while polyhedral (cubic or hexagonal) shapes predominate in the samples with superior photocatalytic activity. From these observations, we concluded, that the shape of the primary particles (both in the case of our home made ones and in various batches of Degussa P25) strongly influence the photocatalytic activity of titania nanoparticles.

1. Introduction

TiO_2 is the most promising candidate for becoming an efficient photocatalyst with wide ranging industrial and household applications [1–5]. The photocatalytic properties of titania are determined by a delicate interplay among a series of structural parameters (*e.g.*, phase composition, size, specific surface area, *etc.*). The role of a given structural feature in photocatalytic performance is difficult to characterize separately, because several of them often change in parallel within a series of samples. On the other hand, because of this multivariable nature of photoactivity, it is of primary importance to develop synthetic methods by which all (or at least some) key structural properties of titania can simultaneously be controlled (for a recent review see Carp et al.[6]).

Flame synthesis (*i.e.*, production of fine particles from gases in flames [7]) is commonly used for producing nanostructured TiO_2. Both pigmentary titania (the world production is *ca.* 2 million tonnes/year [8]) and the benchmark of heterogeneous photocatalysts, Degussa P25 (containing 80–90 wt% anatase and 10–20 wt% rutile; average particle diameter: 35–40 nm (anatase), 85–95 nm (rutile) from XRD and TEM, specific surface area 44–50 $m^2 g^{-1}$ [9]) are manufactured on an industrial scale via this method. During flame synthesis, a liquid containing the Ti(IV) precursor (either organic, *e.g.*, $Ti(OC_3H_7)_4$, or inorganic, *e.g.*, $TiCl_4$) is evaporated or sprayed into a flame, which is made up of H_2 or some hydrocarbon as fuel and O_2 or air as oxidizer. Chemical reactions and particle growth take place extremely fast (<1 s) in typical process conditions. Powders produced in flame reactors are usually aggregates of fine, non-porous primary particles [7]. From the large number of publications in this field, the structure of the TiO_2 thus

* Corresponding author. Tel.: +36 62 544 338; fax: +36 62 420 505.
E-mail address: sipos@chem.u-szeged.hu (P. Sipos).

0926-3373/$ – see front matter © 2008 Elsevier B.V. All rights reserved.
doi:10.1016/j.apcatb.2008.04.018

prepared can be influenced by a variety of process parameters prior to the flame as well as in the flame, of them, the flame temperature and the residence time appear to be the two most important (for the latest review see Ref. [10] and the references cited therein).

Several attempts were made to produce pure (unmodified) titania photocatalysts that are superior to P25, but only a few of them were successful [11–17]. Some bare crystalline TiO_2 with large specific surface area were found to be better than P25 in decomposition of well-adsorbing substrates [11–14], but the multi-step sol–gel route applied and the need of post-synthetic "fine-tuning" make these procedures impractical. Oh et al. obtained titania from thermal plasma, which exhibited excellent performance in acetaldehyde decomposition [15]. Akurati et al. [16] very recently reported a one-step flame synthesis yielding product slightly superior to P25 in methylene-blue degradation. Teoh et al. also employed flame synthesis for preparing an anatase–rutile mixture overtaking P25 in sucrose mineralization [17].

Recently, a co-flow diffusion flame reactor (an in-house modification of a commercially available quartz burner) equipped with a bubble vapor generator has been built in our laboratories. This reactor was used for producing highly photoactive titania, with the strategic aim of developing well-controllable method for obtaining doped TiO_2. This is because in some instances doped titania products synthesized via flame [17] or sol–gel [18,19] technique were found to be significantly better photocatalysts than the identical but non-doped ones. To manufacture bare photocatalysts with maximum photocatalytic performance, a series of samples were produced under controlled conditions, with systematically changing the process parameters, such as fuel/oxidant ratio, fuel/oxidant/precursor feed rates (the detailed analysis of these optimizations will be published elsewhere [20]). It has been observed, that via changing the feed rate of the precursor, the photocatalytic performance of the products (a) varied systematically with the feed rate and (b) in the best cases, the performance of our samples was found to be significantly better than that of P25. In order to reveal the structural feature or features primarily determining the photocatalytic performance, the samples were characterized by XRD, TEM, SEM, HRTEM and specific surface area determination.

2. Experimental

2.1. TiO_2 preparation

The burner of the home made co-flow diffusion flame reactor equipped with a bubble vapor generator is shown in Fig. 1. The quartz-made reactor consists of a central tube through which the precursor ($TiCl_4$, Fluka 99% purity) is fed to the flame via bubbling dry air through it. The flame is air-fed. The fuel (H_2) intake is made through 8 capillaries situated concentrically around the precursor feeding tube. This way the air acts as oxidant and as sheathing gas (similarly to the design described in Ref. [21]). The flow rate of the air was changed between 5070 and 6400 mL/min and the hydrogen flow was kept constant (1230 mL/min). The hydrogen–oxygen molar ratio was set to be near 1:1 (between 1:1 and 1.2:1) in the flame. The flow rate of air bubbling through the $TiCl_4$ was systematically changed between 118 and 355 mL/min. The flow rates were separately controlled with calibrated rotameters (Cole-Parmer). The TiO_2 powder was driven to a conical chimney, which drove the product to a water-cooled glass collector.

2.2. Sample characterization

X-ray diffraction (XRD) measurements were performed on a Philips PW 1820/1830 diffractometer (Cu Kα = 0.15406 nm, 40 kV, and 30 mA, in the $20^\circ \leq 2\Theta \leq 40^\circ$ regime). The average diameters of the particles, (d) were obtained by means of the Scherrer equation [22]

$$d = \frac{k\alpha}{\beta \cos \Theta},$$

where β is the line broadening ($\beta = \beta_S - \beta_0$,, where β_S and β_0 are the half-widths of the XRD peak of the sample and of the silicon standard), k is related to the crystallite shape ($k = 0.9$), and α and Θ are the radiation wavelength and Bragg angle, respectively. A single-crystal silicon standard ($\beta_0 = 0.105^\circ$) was used for calibration. In order to characterize the phase composition of the powders, the diffraction peaks were recorded ($2\Theta = 25.3^\circ$ for anatase (1 0 1) and at $2\Theta = 27.5^\circ$ for rutile (1 1 0)) and integrated. The samples contained anatase and rutile phase only. The weight fraction of rutile, W_R, can be calculated directly from the peak area values by the following equation [23]:

$$W_R = \frac{A_R}{0.884A_A + A_R},$$

where A_R and A_A are the (1 1 0) rutile and the (1 0 1) anatase peak, respectively.

Transmission electron microscopic (TEM) studies were performed to characterize the particle size and size distribution and also to observe the morphology of the particles. TEM micrographs were recorded on a Phillips CM 10 instrument operating at 100 kV using Formvar coated copper grids.

Scanning electron microscopic (SEM) images of selected samples were taken on a Hitachi S4700 scanning electron microscope.

High-resolution transmission electron microscopic (HRTEM) images were recorded on a JEOL-3010 equipment operating at 300 kV and with a point resolution of 0.17 nm. The HRTEM images were used to reveal the crystal structure of individual particles and

Fig. 1. Photograph of the quartz burner of the home made co-flow diffusion flame reactor.

study the possible interparticle connections between particles with different crystal phases.

The specific surface area of the catalysts was determined by nitrogen adsorption at 77 K by a Micromeritics gas adsorption analyzer (Gemini Type 2375), after vacuum drying of the samples at 100 °C for 12 h. The specific surface area was calculated using the BET method.

X-ray photoelectron spectra of selected samples were taken with a SPECS instrument equipped with a PHOIBOS 150 MCD 9 hemispherical electron energy analyzer operated in the FAT mode. The excitation source was the Kα radiation of a magnesium anode ($h\nu$ = 1253.6 eV). The X-ray gun was operated at 180 W power (12 kV, 15mA). The pass energy was set to 20 eV, the step size was 25 meV, and the collection time in one channel was 150 ms. Typically five scans were added to get a single spectrum. The C 1s binding energy of adventitious carbon was used as energy reference: it was taken 285.1 eV. With this method Ti $2p_{3/2}$ spectra were detected at 459 ± 0.2 eV corresponding to Ti^{4+}. For data acquisition both manufacturers (SpecsLab2) and commercial (CasaXPS, Origin) software were used. Before the data analysis X-ray satellites originating from the non-monochromatic excitation source were removed from the spectra.

2.3. Photocatalytic activity measurements

The performance of the catalysts prepared was characterized by using the photocatalytic decomposition of phenol in solution, and methanol, ethanol and acetaldehyde in gas phase, respectively.

For the solution phase experiments, the photoreactor (100 mL) was an open tube with double walls, surrounded by a thermostating jacket (25.0 ± 0.1 °C). The continuously stirred reactor was surrounded and irradiated by six fluorescent lamps (6 W power, radiation maximum at 365 nm, intensity of UV light was $I = 1.02 \pm 0.01 \times 10^{-6}$ einstein s^{-1} measured utilizing ferrioxalate actinometry [24]). The concentration of phenol was measured with an HPLC system consisting of a Merck-Hitachi L-7100 low-pressure gradient pump equipped with a Merck-Hitachi L-4250 UV–vis detector and a Lichrospher RP 18 column applying methanol/water mixture as eluent. Detection wavelength was set at the lower wavelength absorption maximum of phenol (*i.e.*, λ = 210 nm), the high molar absorption coefficient of which makes the detection of small quantities of the substrate possible. Primary degradation products, 1,2- and 1,4-dihydroxy-benzene were also monitored during the analyzes, and it was found, that the concentration profiles of catechol and hydroquinone were similar, as always more hydroquinone was formed. Note that for catalysts of superior performance, the catechol:hydroquinone ratio was much closer to one, than for those with worse activity. The initial concentrations of the substrate was 5.0×10^{-4} M. 1 g L^{-1} photocatalyst concentration was used throughout. No adsorption of phenol was observed on the surface of TiO_2 (even at 4 g L^{-1} photocatalyst loading), therefore the actual concentration of the substrate in the solution phase was regarded to be equal to the concentration of the unreacted phenol. Samples were taken from the suspension in predetermined time intervals, for 120 min. Further details on the experimental set-up can be found elsewhere [25–27].

For the gas phase experiments, 0.100 mL of a suspension containing 300 mg/L of the catalyst was evenly distributed on the surface of glass plates (surface area 3.24 cm^2). The plate was dried in a drying cupboard at 100 °C for 60 min, and was irradiated with UV light for 30 min, and then placed on the bottom of the reaction vessel. A calculated amount of the saturated vapor of the model compound was then injected in the closed reaction vessel of 20 mL volume. The initial concentration of the substrate was 1.2–1.4 × 10^{-4} M. The reaction vessel was irradiated with a fluorescent lamp with a radiation maximum at 365 nm and with an intensity of UV light $I = 7.23 \pm 0.06 \times 10^{-6}$ einstein s^{-1} measured utilizing ferrioxalate actinometry (254 nm ≤ λ ≤ 436 nm) [24]. The concentration of the substrates was measured with a GC system consisting of a HP 5890 gas chromatograph, Supelcovax 10 capillary column (30 m × 0.53 mm, 0.50 μm). For the GC measurements, nitrogen eluent and flame ionization detector was employed.

The initial rate of the photocatalytic degradation of the model compounds, r_0 was considered to be the measure of the efficiency of a given photocatalyst. To determine r_0, an empirical function was fitted to the experimentally observed $c = f(t)$ data points at the conversion range of <60% (in some cases <80%). If the fitting yielded satisfactory description for the data (*i.e.*, $R^2 \geq 0.99$ coefficient of correlation), then the slope of the empirical function at $t = 0$ yields the initial rate of the photocatalytic reaction.

3. Results and discussion

The catalysts prepared were characterized by XRD, specific surface area measurements, transmission and scanning electron microscopy (TEM, HRTEM and SEM). From the XRD patterns (Fig. 2), the phase composition of the crystalline titanium dioxide is 79–98 wt% anatase and the balance is rutile (Table 1). This composition is typical for TiO_2 particles formed in oxygen-rich, vapor-fed [28,29] or spray [30] flames. From XRD line widths, anatase particle diameters are 50–80 nm, but this can only be considered as a first approximation, because of the narrow diffraction peaks observed. Rutile grain sizes are significantly larger than those of anatase (60–200 nm). From the XRD data point of view, the structural differences between the samples prepared are marginal. From the shape of the N_2-adsorption isotherms, as expected [7,10], our samples are not porous. The specific surface areas were found to range between 20 and 32 m^2 g^{-1}. Assuming

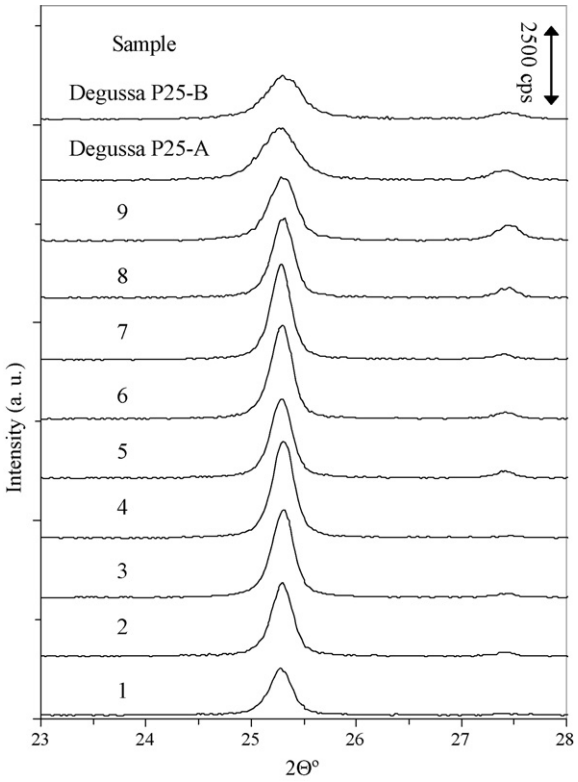

Fig. 2. X-ray diffraction patterns of the flame synthesized samples and that of Degussa P25 (sample A and B) as detailed in Table 1.

Table 1
Structural data and photocatalytic activity of nanocrystalline flame synthesized TiO_2 photocatalysts

Sample no.	Frequency of polyhedral particles (%)	Initial reaction rate of phenol decomposition ($\times 10^{-8}$ M s^{-1})	Anatase to rutile ratio	Primary particle diameter from TEM (nm)	Specific surface area (m^2 g^{-1})	Initial reaction rate/specific surface area × catalyst loading ($\times 10^{-7}$ mol s^{-1} m^{-2})
1	0	7.2	97:3	63	25	2.9
2	10	10.9	96:4	60	20	5.5
3	48	12.8	97:3	54	26	4.9
4	33	11.3	98:2	62	24	4.7
5	59	15.9	92:8	51	28	5.7
6	54	14.9	93:7	58	24	6.2
7	49	15.6	95:5	52	28	5.6
8	69	20.2	89:11	55	27	7.5
9	99	24.2	79:21	48	32	7.6
P25-A	85	11.8	79:21	26	49	2.4
P25-B	100	15.4	89:11	26	50	3.1

that the samples constitute of uniform spheres, an average particle diameter of 50–80 nm can be estimated, in good agreement with those derived from XRD. On the TEM and SEM pictures, particles with diameters similar to those obtained from XRD and N_2-adsorption are seen (Table 1). From the statistical analysis of the TEM images, the samples are moderately polydispersed, *i.e.*, the half-width of the particle size distribution ~20 nm. From these structural data, we concluded, that the systematic variation in the synthesis parameters did not cause any essential change in the structure of the titania prepared.

The photocatalytic performance was tested for phenol decomposition in aerated and near-UV irradiated aqueous solutions and for methanol, ethanol and acetaldehyde decomposition in the gas phase. The initial rate of substrate degradation, r_0, was considered to be the measure of photoactivity. The r_0 values obtained for phenol decomposition exhibited unexpectedly large variations: an almost threefold difference was seen between the highest and the lowest activity catalyst (Fig. 3a Table 1). Similar observations were made for methanol decomposition in the gas phase (Fig. 3b). However, the initial decomposition rates obtained for ethanol and acetaldehyde in the gas phase did not show any major variation: in terms of $r_0 - s$ for these two substrates, our samples were not very different from P25-A and B.

The differences in $r_0 - s$ obtained for the decomposition of phenol and methanol are in particular surprising, as the structural differences between the TiO_2 samples are not large enough to justify such great variation in their photoactivity. Moreover, the r_0 of some of our catalysts (and the r_0 normalized for the specific surface area and catalysts loading for almost all of them) exceeded that of P25 (Table 1). Note that we used P25 from two batches, denoted "A" and "B", respectively. The P25-A had somewhat more rutile content than P25-B (the latter is the recently marketed commercial product); their particle sizes are identical, see Table 1. However, some significant differences are seen in their photoactivity in phenol decomposition: $r_0(A) = 1.18 \times 10^{-7}$ M s^{-1} and $r_0(B) = 1.54 \times 10^{-7}$ M s^{-1}).

Careful inspection of the TEM (Fig. 4) and SEM (Fig. 5) images of the samples led us to the idea, that the differences between $r_0 - s$ are associated with the shape of the titania grains. Samples with the smallest photoactivity contain predominantly spherical particles, while those with the largest r_0 consist almost exclusively polyhedral (faceted) ones (Fig. 4). To express the differences in grain shapes in numerical terms, the TEM images of all the samples prepared were processed in statistical terms. For statistical soundness, 1000–1500 particles were manually counted and measured for each specimen, and samples were taken from at least 10 different regions of the TEM grids. The grains were divided into to groups: spherical and polyhedral (see laid columns in Fig. 4.) A particle was defined to be polyhedral, if it was seen to be terminated mostly by linear sections rather than by arcs on the TEM projection (see enlarged sections in Fig. 4).

There is a clear correspondence between the results of the shape statistics and the samples' photocatalytic activity (Fig. 6): r_0 values for phenol decomposition vary systematically with increasing polyhedral particle count. Shape statistics performed

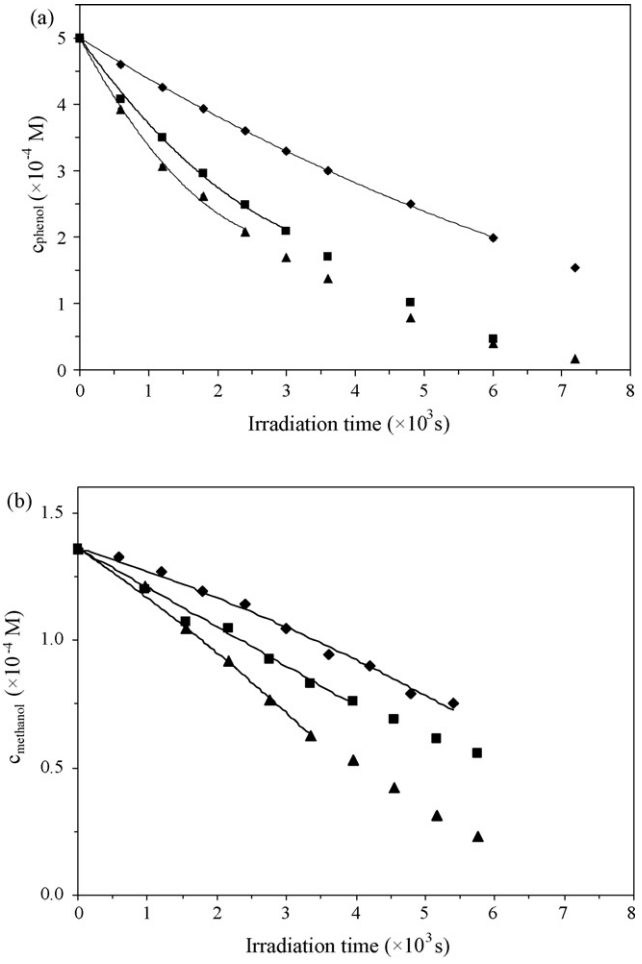

Fig. 3. Photocatalytic decomposition of phenol (a) and methanol (b) on various TiO_2 photocatalysts as a function of reaction time. (▲) sample no. 9; (◆) sample no. 1; (■) Degussa P25-B.

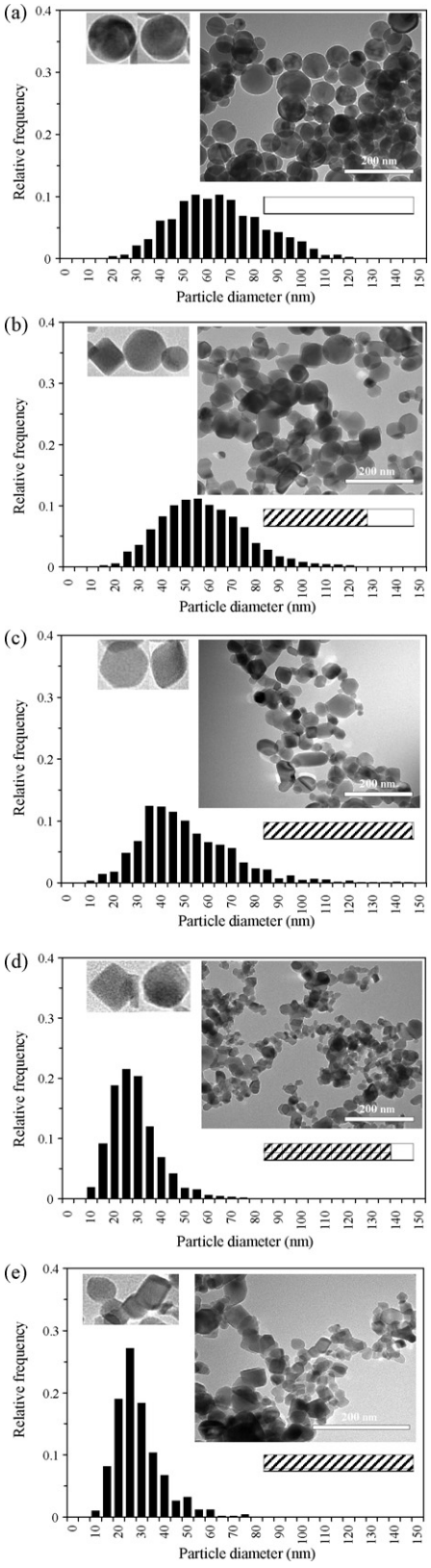

Fig. 4. TEM images and primary particle diameter distributions of some selected photocatalysts. The photocatalytic activity changes in the order (a) < (b) < (c) ((a): sample 1, (b): sample 8 and (c): sample 9 in Table 1). Pictures (d) and (e) correspond to P25-A and P25-B, respectively. The frequency of polyhedral and spherical particles (laid column bar, striped and blank zone, respectively) and the most typical particle shapes are also shown.

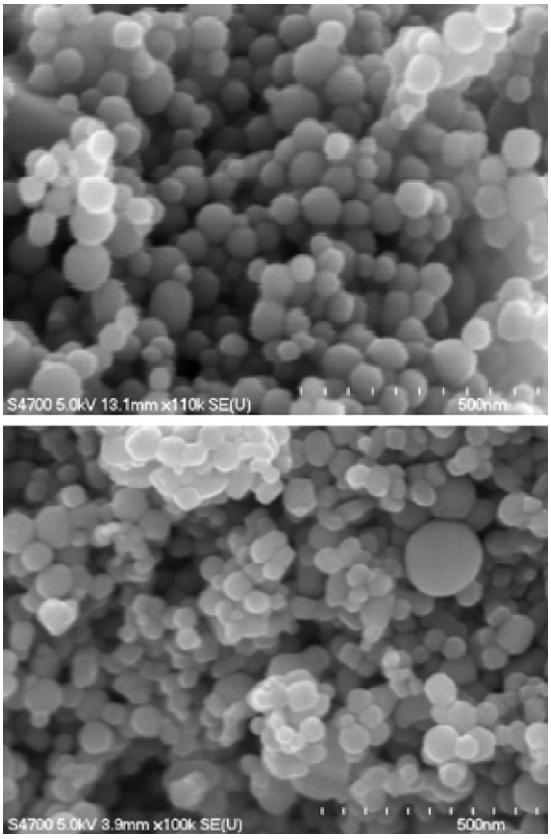

Fig. 5. SEM images of sample no. 1 (upper image) and sample no. 8 (lower image).

on P25-A and B samples led to very similar conclusions: P25-A contained about 85% polyhedral particles, while the P25-B consisted almost no spherical at all. Therefore the difference in shape statistics explains not only the behavior of our samples, but also the significantly better photoactivity of the P25-B sample relative to the P25-A (Figs. 4 and 6). The only structural parameter, which systematically changes in our samples and could have a significant effect on the catalytic activity, is the rutile content, which was claimed to be responsible for the "antenna-effect" [31,32]. However, from HRTEM images (Fig. 7) the rutile and anatase particles in our samples exist as individual single crystals,

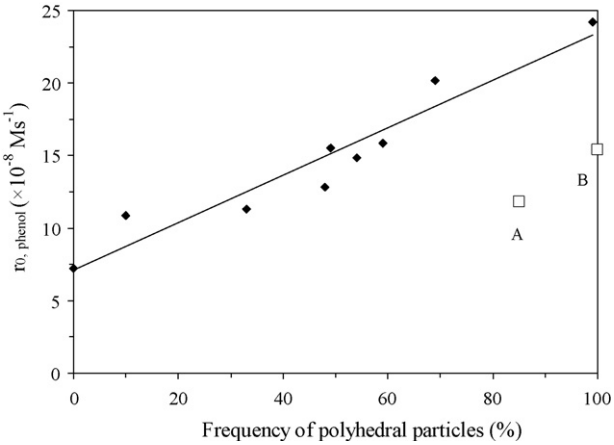

Fig. 6. The initial rate of phenol decomposition plotted as a function of the frequency of particles with polyhedral shape. (◆) our flame synthesized photocatalysts. (□) the two batches (A and B) of Degussa P25.

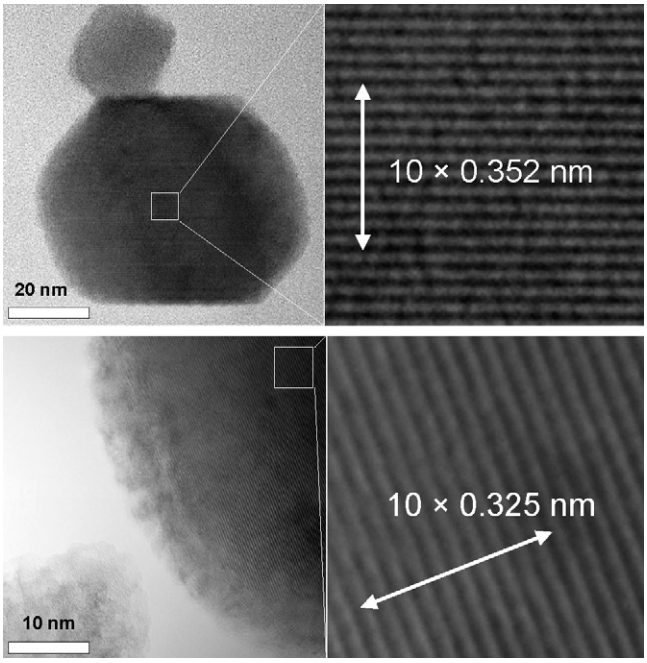

Fig. 7. Upper picture: HRTEM image of an anatase single crystal (periodicity of the (1 0 1) crystal plane is 0.352 nm) in sample 9. Lower picture: HRTEM image of a rutile single crystal (periodicity of the (1 1 0) crystal plane is 0.325 nm) in sample 9.

and not as interwoven rutile–anatase composites as it was claimed [31,32] (but not confirmed by others [33]) for P25.

On the basis of the open literature, flame synthesis procedures produced almost exclusively spherical titania particles [7,10,16,17,28,34,35,21,36–40] and oblong shaped nanocrystals were observed only in a few instances [21,40–43]. Teleki et al. suggested [28] that high temperature residence time of particles enables the growth of large, non-spherical crystals. Akhtar et al. [44] studied the competition between hydrolysis and oxidation (*i.e.*, the one-step formation of the oxide) of $TiCl_4$ and its effects on TiO_2 properties, and stated, that hydrolysis and oxidation dominates at low and high temperatures, respectively, and oxidation results in more faceted particles than spherical ones and enhances the rutile content of the samples. However, if the oxidation of the precursor is carried out very rapidly (*cf.*, using oxygen instead of air as oxidant), spherical TiO_2 particles are formed [7]. It is likely, that in our vapor-fed reactor, with the systematically changing process parameters, the rate of oxidation has significantly changed in the H_2/air flame, which caused the variation in the particle shape.

Sol–gel syntheses yielding monodispersed polyhedral or non-spherical (such as cuboid [45], hexagonal [46] and rod-like [47–50]) TiO_2 nanoparticles are well known from the literature. Photocatalytic tests were performed only for the cuboids [45] and for the rod-like ones [50]. In Ref. [45], the best catalysts exhibited activity equal to that of P25 in methyl orange decomposition. Wahi et al. [51] argued that the difference in the photocatalytic activity of anatase nanorods and nanospheres was due to the difference between the shapes. However, the specimens studied by them were also different in their specific surface area as well as in their particle size. In heterogeneous catalytic processes, it is well known, that the catalytic activity (*i.e.*, the density of catalytically active sites) is crystal face dependent, and is therefore strongly affected by the shape of the catalyst crystals. This is why the fabrication of shape controlled nanocrystals [51] for catalytic purposes and their characterization [52–55] can still be considered as a hot topic in nanoscience. In a very recent paper, for example, polyhedral Pt-nanocrystals were described to exhibit electrocatalytic activity far better than that of spherical ones, from which they were manufactured [56]. However, to the best of our knowledge, such shape dependent phenomenon for heterogeneous photocatalytic processes has not yet been described.

According to Ardizzone et al., [57], photocatalytic activity of nanocrystalline TiO_2 samples clearly correlates with the density of the surface OH groups: the best photocatalysts were found to be the ones showing the largest OH/O_{TOT} surface ratio. The two kinds of components discussed in Ref. [57] (*i.e.*, lattice oxygen with binding energy around 530 eV and the oxygen of the OH groups around 532 eV) were also identified in our samples. Within the error of the method, the ratios of the hydroxylic and lattice oxygen for P25-A and B, and for our samples displaying inferior photocatalytic activity were practically the same (*ca.* 0.14). However, for our best photocatalysts, this ratio was found to be smaller (*ca.* 0.04). Therefore, the population of the OH groups on the surface is unlikely to be responsible for the enhanced photocatalytic activity observed for our photocatalysts. It has to be noted here, however, that fitting the spectrum of the better quality photocatalysts by using only two components gave a very poor fit, especially on the low binding energy side of the spectrum. For obtaining satisfactory fitting, a third, low energy component had to be assumed with a maximum around 529 eV. It is not clear at present, if this third type of oxygen (if it exists at all) is somehow associated with the enhanced photocatalytic activity, to unambiguously prove this, further experiments on a significantly larger number of samples is necessary.

At this moment, one can only speculate, why faceted particles are superior to spherical ones in phenol and methanol decomposition. Activity could be governed by the crystal face dependent number (or density) of recombination centres or by the anisotropic charge transport in TiO_2 [5]. A further possible explanation involves the differences in O_2-adsorption capacity or surface properties related to substrate/intermediate chemisorption. Whichever it is, optimization of TiO_2-syntheses to yield faceted nanocrystals appears to be a promising way of producing photocatalysts (both bare and doped) with significantly enhanced photocatalytic activity.

4. Conclusion

A series of titania nanoparticles with practically identical structure but widely different photocatalytic activity were synthesized. The particle shape was found to play crucial role in the photocatalytic activity: specimens with only polyhedral (faceted) nanocrystals were found to be significantly better in photocatalytic decomposition of phenol and methanol than those containing a mixture of spherical and polyhedral ones. Our results also explain why the recently marketed, purely polyhedral Degussa P25 samples are superior to the previous batches, which contain a mixture of spherical and polyhedral nanocrystals.

Acknowledgements

This work was supported by the Hungarian National Office of Research and Technology (NKTH) and the Agency for Research Fund Management and Research Exploitation (KPI) under contract no. RET-07/2005 by the OTKA (67559) and by the GVOP (GVOP-3112004-05-0259/3.0). K.M. thanks the Magyary Zoltán Foundation for its financial support. The authors thank Dr. István Pálinkó for his helpful advise and Dr. Lajos Tóth for the HRTEM analysis.

References

[1] A. Fujishima, K. Honda, Nature 238 (1972) 37.
[2] A. Fujishima, T.N. Rao, D. Tryk, J. Photochem. Photobiol. C: Photochem. Rev. 1 (2000) 1.
[3] B. Oregan, M. Grätzel, Nature 353 (1991) 737.
[4] L. Kőrösi, A. Oszkó, G. Galbács, A. Richardt, V. Zöllmer, I. Dékány, Appl. Catal. B: Environ. 77 (2007) 175.
[5] U. Diebold, Surf. Sci. Rep. 48 (2003) 53.
[6] O. Carp, C.L. Huisman, A. Reller, Prog. Solid State Chem. 32 (2004) 33.
[7] S.E. Pratsinis, Prog. Energy Combust. Sci. 24 (1998) 197.
[8] J.H. Braun, J. Coat. Technol. 69 (1997) 72.
[9] Z. Zhang, C.-C. Wang, R. Zakaria, J.Y. Ying, J. Phys. Chem. B 102 (1998) 10871.
[10] R. Strobel, A. Baiker, S.E. Pratsinis, Adv. Powder Technol. 17 (2006) 457.
[11] Y. Xie, C. Yuan, J. Mol. Catal. A: Chem. 206 (2003) 419.
[12] S.J. Kim, E.G. Lee, S.D. Park, C.J. Jeon, Y.H. Cho, C.K. Rhee, W.W. Kim, J. Sol–Gel Sci. Technol. 22 (2001) 63.
[13] H. Kominami, H. Kumamoto, Y. Kera, B. Ohtani, J. Photochem. Photobiol.A: Chem. 160 (2002) 99.
[14] G. Dagan, M. Tomkiewicz, J. Phys. Chem. 97 (1993) 12651.
[15] S.-M. Oh, S.-S. Kim, J.E. Lee, T. Ishigaki, D.-W. Park, Thin Solid Films 435 (2003) 252.
[16] K.K. Akurati, A. Vital, G. Fortunato, R. Hany, F. Nueesch, T. Graule, Solid State Sci. 9 (2007) 247.
[17] W.Y. Teoh, L. Madler, D. Beydoun, S.E. Pratsinis, R. Amal, Chem. Eng. Sci. 60 (2005) 5852.
[18] M. Zhou, J. Yu, B. Cheng, J. Hazard. Mater. B137 (2006) 1838.
[19] J. Zhu, F. Chen, J. Zhang, H. Chen, M. Anpo, J. Photochem. Photobiol. A: Chem. 180 (2006) 196.
[20] N. Balázs, P. Sipos, A. Dombi, K. Mogyorósi, in preparation.
[21] Y. Zhao, C. Li, X. Liu, F. Gu, H. Jiang, W. Shao, L. Zhang, Y. He, Mater. Lett. 61 (2007) 79.
[22] B.D. Cullity, Elements of X-ray Diffraction, Addison-Wesley, Reading, 1978.
[23] H. Zhang, J.F. Banfield, J. Phys. Chem. B 104 (2000) 3481.
[24] C.G. Hatchard, C.A. Parker, Proc. R. Soc. A-Math. Phy. 235 (1956) 518.
[25] I. Ilisz, Zs. László, A. Dombi, Appl. Catal. A: Gen. 180 (1999) 25.
[26] I. Ilisz, A. Dombi, Appl. Catal. A: Gen. 180 (1999) 35.
[27] A. Dombi, I. Ilisz, Zs. László, Gy. Wittmann, Ozone Sci. Eng. 24 (2002) 49.
[28] A. Teleki, S.E. Pratsinis, K. Kalyanasundaram, P.I. Gouma, Sens. Actuators B 119 (2006) 683.
[29] A. Teleki, S.E. Pratsinis, K. Wegner, R. Jossen, F. Krumeich, J. Mater. Res. 20 (2005) 1336.
[30] H. Schulz, L. Madler, R. Strobel, R. Jossen, S.E. Pratsinis, T. Johannessen, J. Mater. Res. 20 (2005) 2568.
[31] D.C. Hurum, A.G. Agrios, K.A. Gray, T. Rajh, M.C. Thurnauer, J. Phys. Chem. B 107 (2003) 4545.
[32] D.C. Hurum, K.A. Gray, T. Rajh, M.C. Thurnauer, J. Phys. Chem. B 109 (2005) 977.
[33] A.K. Datye, G. Riegel, J.R. Bolton, M. Huang, M.R. Prairie, J. Solid State Chem. 115 (1995) 236.
[34] J.R. McCormick, B. Zhao, S.A. Rykov, H. Wang, J.G. Chen, J. Phys. Chem. B 108 (2004) 17398.
[35] C. Almquist, P. Biswas, J. Catal. 212 (2002) 145.
[36] H.K. Kammler, S.E. Pratsinis, P.W. Morrison Jr., B. Hemmerling, Combust. Flame 128 (2002) 369.
[37] W.Y. Teoh, R. Amal, L. Madler, S.E. Pratsinis, Catal. Today 120 (2007) 203.
[38] K.K. Akurati, A. Vital, U.E. Klotz, B. Bommer, T. Graule, M. Winterer, Powder Technol. 165 (2006) 73.
[39] O.I. Arabi-Katbi, S.E. Pratsinis, P.W. Morrison Jr., C.M. Megaridis, Combust. Flame 124 (2001) 560.
[40] O.I. Arabi-Katbi, K. Wegner, S.E. Pratsinis, Ann. Chim. Sci. Mat. 27 (2002) 37.
[41] H.D. Jang, S.-K. Kim, Mat. Res. Bull. 36 (2001) 627.
[42] G. Skandan, Y.-J. Chen, N. Glumac, B.H. Kear, Nanostruct. Mater. 11 (1999) 149.
[43] Y. Zhao, C. Li, X. Liu, F. Gu, H. Jiang, W. Shao, L. Zhang, Y. He, Mater. Lett. 61 (2007) 73.
[44] M.K. Akhtar, S. Vemury, S.E. Pratsinis, AIChE J. 40 (1994) 1183.
[45] H. Wang, Y. Wu, B.-Q. Xu, Appl. Catal. B: Environ. 59 (2005) 139.
[46] T. Morris, J. Reiss, K. Diesner, D. Su, A. Chemseddine, J. Phys. Chem. B 101 (1997) 8052.
[47] B. Koo, J. Park, Y. Kim, S.-H. Choi, Y. -E- Sung, T. Hyeon, J. Phys. Chem. B 110 (2006) 24318.
[48] Y. Jun, M.F. Casula, J.-H. Sim, S.Y. Kim, J. Cheon, A.P. Alivisatos, J. Am. Chem. Soc. 125 (2003) 15981.
[49] P.D. Cozzoli, A. Kornowski, H. Weller, J. Am. Chem. Soc. 125 (2003) 14359.
[50] Y. Yun, J.-H. Lee, J. Choi, J. Cheon, J. Phys. Chem. B 109 (2005) 14795.
[51] R.K. Wahi, W.W. Yu, Y. Liu, M.L. Mjia, J.C. Falkner, W. Nolte, V.L. Colvin, J. Mol. Catal. A: Chem. 242 (2005) 48.
[52] T. Schalow, B. Brandt, D.E. Starr, M. Laurin, S.K. Shaikhutdinov, S. Schauermann, J. Libuda, H.-J. Freund, Angew. Chem. Int. Ed. 45 (2006) 3693.
[53] A.M. Doyle, S.K. Shaikhutdinov, S.D. Jackson, H.-J. Freund, Angew. Chem. Int. Ed. 42 (2003) 5240.
[54] B. Veisz, Z. Király, L. Tóth, B. Pécz, Chem. Mater. 14 (2002) 2882.
[55] B. Veisz, Z. Király, Langmuir 19 (2003) 4817.
[56] N. Tian, Z.-Y. Zhu, S.-G. Sun, Y. Ding, Z.L. Wang, Science 316 (2007) 732.
[57] S. Ardizzone, C.L. Bianchi, G. Cappelletti, S. Gialanella, C. Pirola, V. Ragaini, J. Phys. Chem. C 111 (2007) 13222.